

RESEARCH ARTICLE | APRIL 24 2024

AlGaN/GaN MOS-HEMT enabled optoelectronic artificial synaptic devices for neuromorphic computing ^{EP}

Jiaxiang Chen ; Haitao Du ; Haolan Qu ; Han Gao ; Yitian Gu ; Yitai Zhu ; Wenbo Ye ; Jun Zou; Hongzhi Wang ; Xinbo Zou  



APL Mach. Learn. 2, 026113 (2024)

<https://doi.org/10.1063/5.0194083>

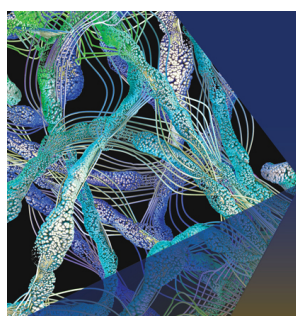


View
Online



Export
Citation

23 July 2024 07:57:25



The Journal of Chemical Physics

Special Topic:

Machine Learning for Biomolecular Modeling

Guest Editors: Pratyush Tiwary, Francesca Grisoni, Pilar Cossio

Submit Today!

AlGaN/GaN MOS-HEMT enabled optoelectronic artificial synaptic devices for neuromorphic computing

Cite as: APL Mach. Learn. 2, 026113 (2024); doi: 10.1063/5.0194083

Submitted: 25 December 2023 • Accepted: 8 April 2024 •

Published Online: 24 April 2024



View Online



Export Citation



CrossMark

Jiaxiang Chen,^{1,2,3}  Haitao Du,^{1,2,3}  Haolan Qu,^{1,2,3}  Han Gao,^{1,2,3}  Yitian Gu,^{1,2,3}  Yitai Zhu,^{1,2,3} 
Wenbo Ye,^{1,2,3}  Jun Zou,⁴ Hongzhi Wang,⁵  and Xinbo Zou^{1,6,a)} 

AFFILIATIONS

¹School of Information Science and Technology, ShanghaiTech University, Shanghai 201210, China

²Shanghai Institute of Microsystem and Information Technology, Chinese Academy of Sciences, Shanghai 200050, China

³University of Chinese Academy of Sciences, Beijing 100049, China

⁴School of Science, Shanghai Institute of Technology, Shanghai 201418, China

⁵College of Materials Science and Engineering, Donghua University, 201620 Shanghai, China

⁶Shanghai Engineering Research Center of Energy Efficient and Custom AI IC, Shanghai 200031, China

^{a)} Author to whom correspondence should be addressed: zouxb@shanghaitech.edu.cn

ABSTRACT

Artificial optoelectronic synaptic transistors have attracted extensive research interest as an essential component for neuromorphic computing systems and brain emulation applications. However, performance challenges still remain for synaptic devices, including low energy consumption, high integration density, and flexible modulation. Employing trapping and detrapping relaxation, a novel optically stimulated synaptic transistor enabled by the AlGaN/GaN hetero-structure metal-oxide semiconductor high-electron-mobility transistor has been successfully demonstrated in this study. Synaptic functions, including excitatory postsynaptic current (EPSC), paired-pulse facilitation index, and transition from short-term memory to long-term memory, are well mimicked and explicitly investigated. In a single EPSC event, the AlGaN/GaN synaptic transistor shows the characteristics of low energy consumption and a high signal-to-noise ratio. The EPSC of the synaptic transistor can be synergistically modulated by both optical stimulation and gate/drain bias. Moreover, utilizing a convolution neural network, hand-written digit images were used to verify the data preprocessing capability for neuromorphic computing applications.

© 2024 Author(s). All article content, except where otherwise noted, is licensed under a Creative Commons Attribution (CC BY) license (<https://creativecommons.org/licenses/by/4.0/>). <https://doi.org/10.1063/5.0194083>

I. INTRODUCTION

Neuromorphic processors hold the merits of high energy efficiency, outstanding fault tolerance, and compact size for complex computing scenarios, where bottlenecks in speed and power consumption start to show up in von Neumann computing architecture.¹⁻³ Recently, human brain inspired neuromorphic computing has attracted extensive research attention owing to its real-time analysis of unstructured information,⁴ low power consumption, and parallel data processing capabilities.⁵⁻⁹ In the human brain, the vast number of synapses ($\sim 10^{15}$) play a signif-

icant role in the neural network that processes and encodes the received information.^{10,11} In addition to electrically triggered synaptic devices,¹² research on optoelectronic synaptic devices indicates the promise of parallel multiple-input, wide bandwidth, and low crosstalk, suggesting great potential in artificial intelligence (AI) implementations and neuromorphic computing.^{13,14} When being exposed to optical excitation, classical synaptic reactions have been successfully emulated, including excitatory postsynaptic current (EPSC), paired-pulse facilitation (PPF), short-term memory/long-term memory (STM/LTM), and spike-timing-dependent plasticity (STDP).¹⁵

Recently, extensive efforts have been put into the implementation of artificial synaptic devices using various emerging materials.¹⁶ Silicon (Si)-based artificial synaptic devices and neuromorphic computing systems have been successfully demonstrated.^{15,17} In addition, oxide-based devices, for instance, a chitosan-gated indium tin oxide (ITO) phototransistor was used to mimic the synaptic functions by the photonic synergic coupling effects, but this synapse showed the relatively high energy consumption of 3.92 μJ .^{18,19} Two-dimensional material based devices have also been demonstrated as artificial synapses.^{20–22} For example, a two-terminal electronic synapse based on multilayer hexagonal boron nitride (h-BN) as a resistive switching medium shows good emulation of synaptic functions, including STM and LTM.²² Despite steady progress presented by low-dimensional materials and associated two-terminal synaptic devices, limited flexibility in terms of gate control capability and susceptibility to high temperature still remain a challenge. In addition, III-nitride wide-bandgap materials, such as aluminum nitride (AlN)^{5,23} and gallium nitride (GaN),²⁴ are promising materials for achieving artificial optoelectronic synaptic functions owing to their direct bandgap and persistent photoconductivity.²⁵ AlGaIn/GaN metal-oxide semiconductor high-electron-mobility transistors (MOS-HEMTs) on Si have reportedly shown low gate leakage current, high signal-to-noise ratio (SNR), flexible modulation, CMOS compatibility, and large-scale integration potential. Compared to two-terminal devices, employment of transistors to mimic the biological nervous system holds the advantages of synergistic modulation of the channel current by both incident light and gate/drain bias.¹⁸ In AlGaIn/GaN MOS-HEMTs, the trap states induced charge trapping/detrapping process and drain current transient response have been investigated in our previous studies.^{26–28} In response to optical excitation, the traps in the dielectric layer or the AlGaIn/GaN channel may release photoexcited charges and lead to current response, which has a great potential to mimic synaptic plasticity.^{5,29} The low amplitude of trap-induced transient current in the turned-off AlGaIn/GaN MOS-HEMTs promised the virtue of low energy consumption.^{28,30} Therefore, AlGaIn/GaN-based MOS-HEMTs on the Si substrate represent a promising artificial synaptic candidate for large-scale integrated neuromorphic computing.

In this study, we demonstrate an optical-stimulated artificial synaptic device based on AlGaIn/GaN MOS-HEMT, which emulates various biological synaptic functions. By applying an optical spike, the AlGaIn/GaN MOS-HEMTs exhibit low energy consumption and high SNR in a single EPSC event. The short- and long-term synaptic plasticities with multiple optical spikes have been demonstrated, while responses to gate and drain voltage are also investigated. In addition, data processing in various applications exhibits a substantial amount of redundancy, resulting in detrimental consequences, such as decreased processing speed and enlarged power consumption.³¹ Consequently, the demand for a synaptic device capable of preprocessing data combined with advanced machine learning algorithms while maintaining accuracy has become imperative. The data preprocessing ability of the proposed synaptic device is validated by digit image recognition via convolution neural network (CNN). The proposed AlGaIn/GaN synaptic transistors hold great potential for applications, including visual neuromorphic computing platforms and data-intensive machine learning.

II. FABRICATED SYNAPTIC DEVICE STRUCTURE FOR NEUROMORPHIC COMPUTING

The AlGaIn/GaN heterostructure MOS-HEMT as a three-terminal synaptic device investigated in this study was epitaxially grown on a 6 in. Si substrate using metal-organic chemical vapor deposition (MOCVD). The epitaxial layers of the GaN-based synapse device consisted of a 3 μm thick buffer layer, a 200 nm undoped GaN channel layer, a 1 nm AlN spacer layer, a 25 nm undoped $\text{Al}_{0.25}\text{Ga}_{0.75}\text{N}$ layer, and a 3 nm GaN cap layer. To achieve mesa isolation, the device was etched by BCl_3/Cl_2 -based inductively coupled plasma reactive ion etching (ICP-RIE). Subsequently, the source and drain regions were deposited using a Ti/Al/Ni/Au (20/150/50/80 nm) ohmic metal stack, followed by rapid thermal annealing at 850 $^\circ\text{C}$ for 40 s with a nitrogen (N_2) ambient. To mitigate the leakage current, three cycles of treatments were applied to the device surface, which included 100 W O_2 plasma oxidation for 1 min and HCl immersion cleaning for 2 min in each cycle. A 15 nm Al_2O_3 dielectric layer was immediately deposited by using plasma-enhanced atomic layer deposition (PEALD) at 150 $^\circ\text{C}$, which served as both the dielectric and passivation layer for access regions. Finally, the gate electrode was formed by Ni/Au (20/200 nm) metal deposition. The device in this work featured a gate length (L_G), a gate-source distance (L_{GS}), a gate-drain distance (L_{GD}), and a gate width (W_G) of 1, 2, 3, and 20 μm , respectively. The AlGaIn/GaN MOS-HEMT on the Si substrate shows great potential for integration of neuromorphic computing devices with Si CMOS circuits, which could provide additional benefits, such as increased density, reduced cost, and multiple functions.³² A representative scanning electron microscopy (SEM) image of the fabricated AlGaIn/GaN MOS-HEMT is shown in Fig. 1(a). The enlarged SEM image is shown in Fig. 1(b). The transfer I_{DS} - V_{GS} characteristics of MOS-HEMT at various V_{DS} from 0.5 to 3.0 V are shown in Fig. 1(c). Using the 1 mA/mm standard, the threshold voltage (V_{TH}) is extracted from the transfer curves to be -5.3 V at $V_{DS} = 0.5$ V. The on-off ratio of 10^9 is achieved, indicating outstanding charge modulation of the MOS gate structures. The device exhibits a low leakage current of 7.1 nA/mm at V_{GS} of -10 V and V_{DS} of 3 V. The output characteristics of AlGaIn/GaN MOS-HEMT are shown in Fig. 1(d). The drain current density reaches a maximum value of 534 mA/mm at $V_{GS} = -1$ V.

III. RESULT AND DISCUSSION

Figure 2(a) shows the typical biological synapse, which holds importance within the biological nervous system since it serves as a vital block facilitating signal transmission between adjacent neurons. Upon stimulus of the biological pre-synapse, the presynaptic membrane will immediately trigger the exocytosis of neurotransmitters into the synaptic cleft.³³ Then, the receptor on the postsynaptic neuron membrane opens the channel to realize the signal transmission, and the strength of signal transmission represents the weight of the synapse. The connections between a pair of neurons are modulated by synaptic weights, which also determine the information from the previous neuron transmitted to the next neuron. For AlGaIn/GaN MOS-HEMT, the gate electrode, two-dimensional electron gas (2DEG) channel with source/drain electrodes, and channel current are considered as pre-synapse,

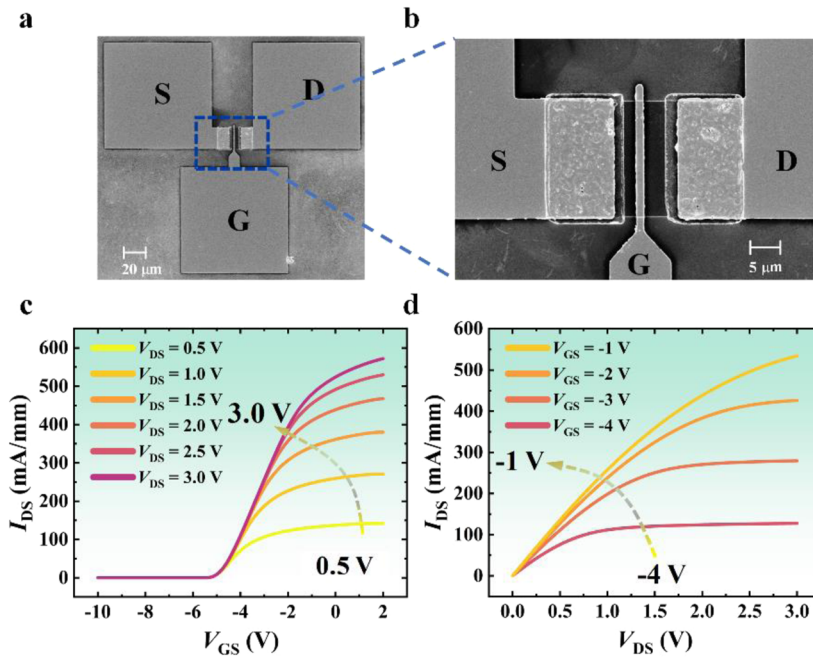


FIG. 1. (a) A representative SEM image of the AlGaIn/GaN MOS-HEMT synaptic device. (b) The enlarged SEM image of the device. At room temperature, (c) transfer characteristics, and (d) output characteristics of synaptic devices.

post-synapse, and postsynaptic current, respectively.³⁴ The wavelength of the monochromatic optical light is 405 nm with an output power of 10 mW as an optical excitation. The optical spikes were applied on the AlGaIn/GaN synaptic device, while the photogenerated carriers represent synapse transmitters, and the drain current is used to transport these transmitters.

Due to the piezoelectric polarization and spontaneous polarization effects of nitride materials, the 2DEG was formed at the AlGaIn/GaN heterointerface, leading to a normally on AlGaIn/GaN MOS-HEMT.^{26,35} As shown in Fig. 2(b), when applying a negative V_{GS} below V_{TH} , the MOS-HEMT device is turned off. With an optical excitation, the trap levels within the AlGaIn/GaN channel region will absorb light energy to excite the carriers, which contribute to the transient accumulation in the channel, forming the sharp increase in the current signal. Subsequently, the transverse electrical field leads to the collection of photoexcited carriers within the channel, resulting in a reduction in the current toward equilibrium. The overall current response in the device can be extracted as excitatory postsynaptic currents (EPSCs) shown in Fig. 2(c). EPSCs were triggered by presynaptic optical spiking with a 405 nm wavelength and 200 ms pulse duration, the amplitude of which serves as the indicator of the output for artificial synapse. The measured gate and drain bias were set as -8 and 0.5 V, respectively. With a 405 nm optical spike applied, the peak current amplitude of 983 nA is obtained from the drain current level of 5 nA before the spike. When the optical excitation is switched off, a gradual decay of the EPSC current is observed after a sharp increase in current, indicating that the optoelectronic synapse generating the response resembles a biological EPSC signal.

The optical pulse duration dependent EPSC and energy consumption were extracted and shown in Fig. 2(d). The blue data points represent the peak EPSC value as a function of the optical pulse duration. With increasing optical pulse duration, the amplitude of EPSC first increases and then reaches the saturation. The energy consumption of the single EPSC event with an optical spike duration by^{13,36}

$$dE = V_{DS} \times I_{DS} \times dt, \tag{1}$$

where I_{DS} and t are the peak EPSC value and optical pulse duration, respectively.²⁴ The energy consumption could be reduced by decreasing t , where the shorter t will generate small I_{DS} . Thus, the reduction in the optical pulse duration is an effective way to lower the energy consumption of the synaptic device. Energy consumption was reduced from 171.8 nJ to 34.2 pJ with a decrease in the optical spike duration from 300 to 3 ms. The SNR of the EPSC signal can be determined by the following equation:¹¹

$$SNR \geq 10 \lg \left(\frac{P_S}{P_N} \right) \approx 10 \lg \left(\frac{A_{EPSC}}{\sigma_{Noise}} \right), \tag{2}$$

where P_S , P_N , A_{EPSC} , and σ_{Noise} are the mean power of the EPSC, mean power of the noise, the amplitude of EPSC, and the standard deviation of the noise current, respectively. Thus, the SNR was increased from 15.03 dB (at an interval time of 50 ms) to 20.75 dB (at an interval time of 1000 ms), showing a good SNR of the EPSC signal. In addition, writing and erasing characteristics (Fig. S1, supplementary material) show the good cycling endurance of the III-N synaptic devices.

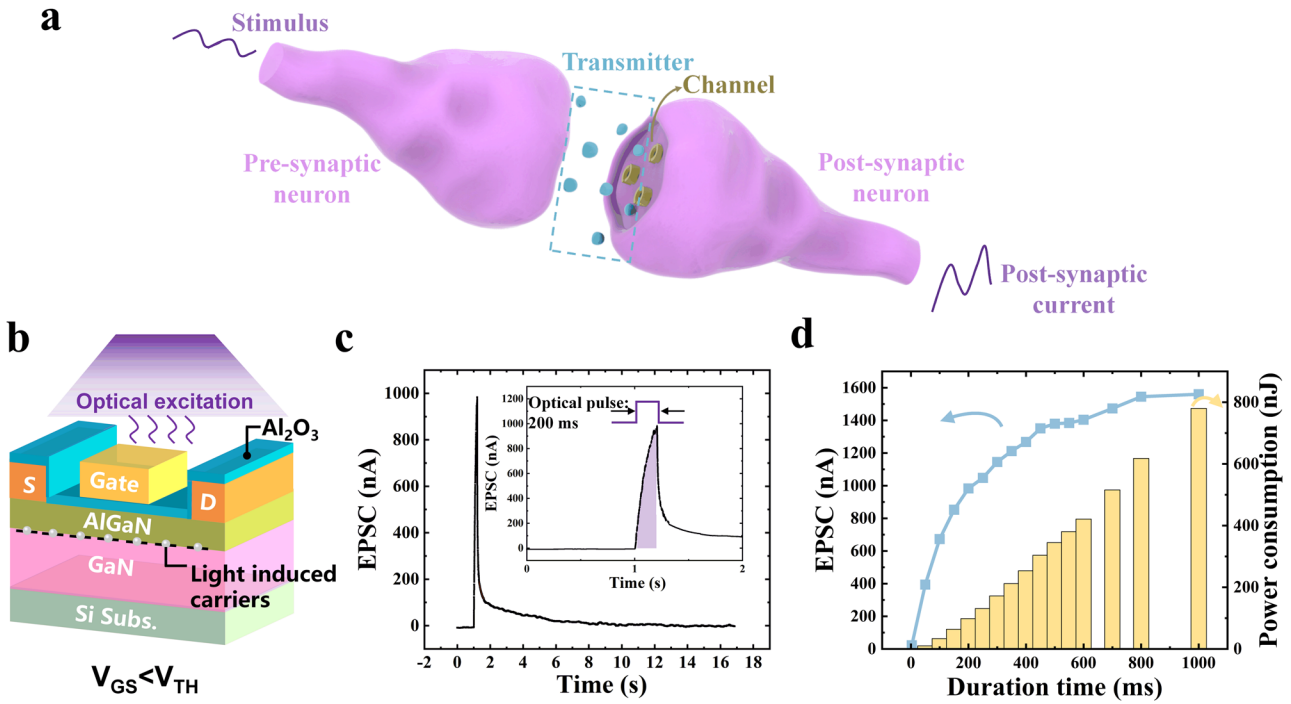


FIG. 2. Schematic of (a) the biological synapse and (b) the light-triggered detrapping process. (c) Excitatory postsynaptic current (EPSC) with a single optical pulse of 200 ms. Inset shows the enlarged EPSC current and optical pulse duration. (d) Peak EPSC value and energy consumption as functions of optical pulse duration.

The temporal potentiation of synaptic connection is known as short-term plasticity (STP) in neuroscience.³⁷ PPF as a representative STP indicates the receptivity of biological synapses for temporal information processing, such as visual and auditory signals in biology.^{34,38} Specifically, PPF refers to the stimulus immediately after the previous pulse, which will evoke a larger EPSC than the previous one. Figure 3(a) shows the schematic of PPF in a nervous system, and when the presynaptic neuron is triggered by two close pulses, the residual Ca^{2+} from the first pulse enables more transmitter release, leading to an enhanced response.³⁹ In Fig. 3(b), to mimic the biological synaptic functions, the PPF response was monitored by applying two adjacent optical excitations with the pulse duration of 300 ms and pulse interval of 250 ms, while the bias condition is the same as the EPSC measurement. In the PPF, when the first optical spike was applied, the photogenerated electrons move into the 2DEG channel, resulting in the signal peak current A_1 of EPSC. When the first spike was switched-off, the carriers trapped at the shallow trap could be released, leading to the decay process of EPSC. If the AlGaIn/GaN synaptic transistor is optically stimulated again before the complete release of the trapped photogenerated carriers, traps with even lower activation energy would be occupied by the carriers, and then, the EPSC was enhanced with the second peak current A_2 . The release process of the excess trapped carriers gives rise to longer decay time as the mimicking of PPF. This PPF manifestation is also similar to the process of excitatory signals originating from the presynaptic membrane to the postsynaptic membrane with two consecutive stimulations in the biological nervous system, and

the A_1 and A_2 were extracted to be 1122 and 1408 nA, respectively. Meanwhile, the device-to-device (Fig. S2, supplementary material) and cycle-to-cycle (Fig. S3, supplementary material) measurements for EPSC and PPF show that the synaptic devices have excellent spatial and temporal uniformities.

The PPF index was defined as the ratio of the second EPSC current response to the first EPSC current response (A_2/A_1),²³ which was also measured for varying interval times (Δt) from 250 ms to 16 s, as shown in Fig. 3(b). The PPF index first decreases promptly and then gradually when the Δt increases. The interval time-dependent PPF index phenomenon can be well described by the following equation:^{5,40}

$$PPF = 1 + C_1 \exp\left(-\frac{\Delta t}{\tau_1}\right) + C_2 \exp\left(-\frac{\Delta t}{\tau_2}\right), \quad (3)$$

where C_1 and C_2 indicate the ratio of the current magnitudes in two stages, respectively. τ_1 and τ_2 represent the characteristic relaxation times of fast and slow phases, respectively. The fitting curve of PPF is shown as a dashed line in Fig. 3(b). From the fitting results, τ_1 , τ_2 , C_1 , and C_2 were extracted as 124.6 ms, 35.2 s, 0.44, and 0.197, respectively. For the PPF index, τ_2 is longer than τ_1 , showing good short-term memory like a biological synapse. As Δt increases, the extent of the PPF enhancement is plotted from 125.5% to 113.1%, which is mainly due to the photogenerated carriers excited by the previous optical pulse being gradually emitting

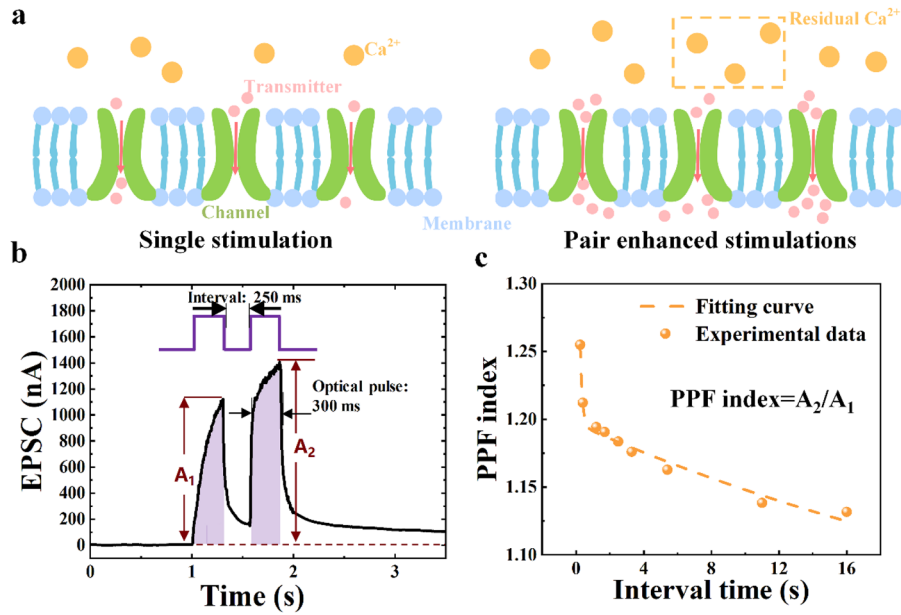


FIG. 3. (a) Schematic of the pair-pulse facilitation (PPF) induced by residual calcium ions (Ca^{2+}) in a nervous system. (b) Typical PPF response of the AlGaIn/GaN MOS-HEMT with adjacent applied pulses. (c) The amplitude of PPF as a function of the double-pulse interval between two sequential pulses.

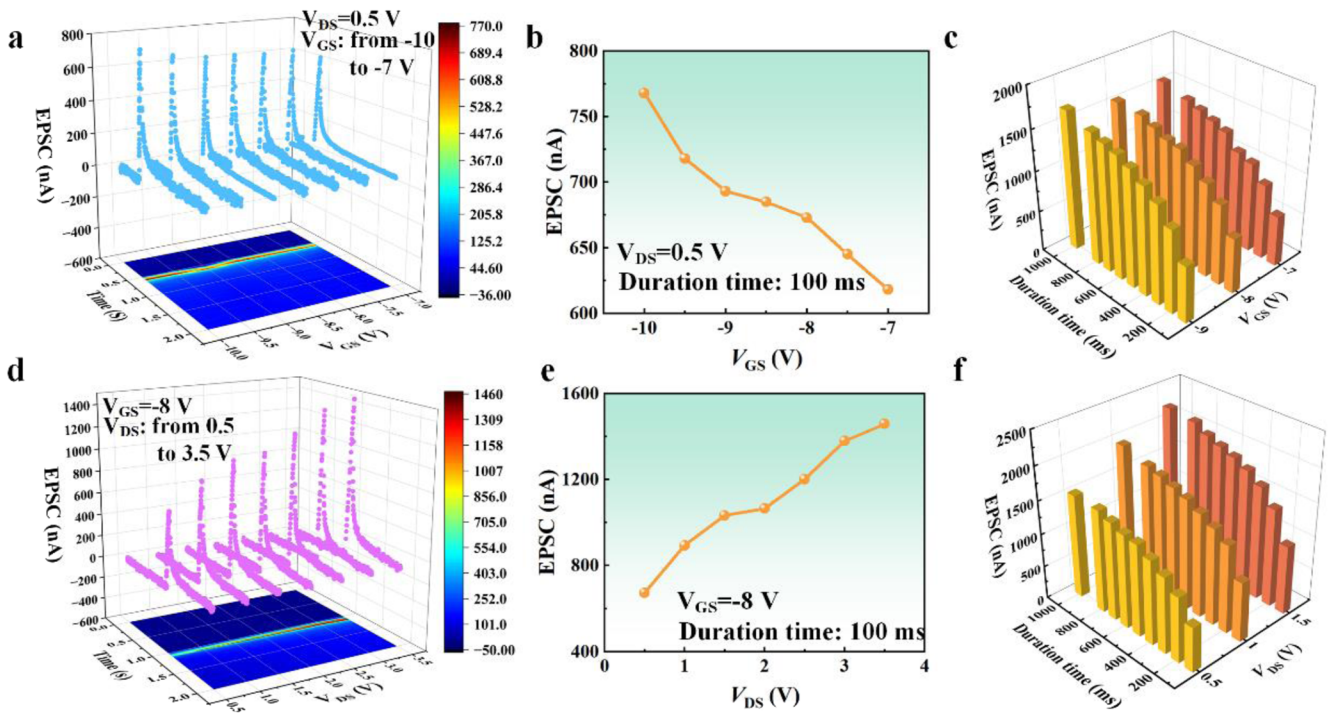


FIG. 4. (a) EPSC at various V_{GS} with V_{DS} of 0.5 V. (b) Gate voltage dependence of the EPSC amplitude with an optical spike duration of 100 ms. (c) Amplitude of EPSC with various V_{GS} at fixed V_{DS} of 0.5 V. (d) EPSC at various V_{DS} with V_{GS} of -8 V. (e) Drain voltage dependence of the EPSC amplitude at the optical spike duration of 100 ms. (f) EPSC at different drain voltage V_{DS} with a fixed V_{GS} of -8 V.

23 July 2024 07:57:25

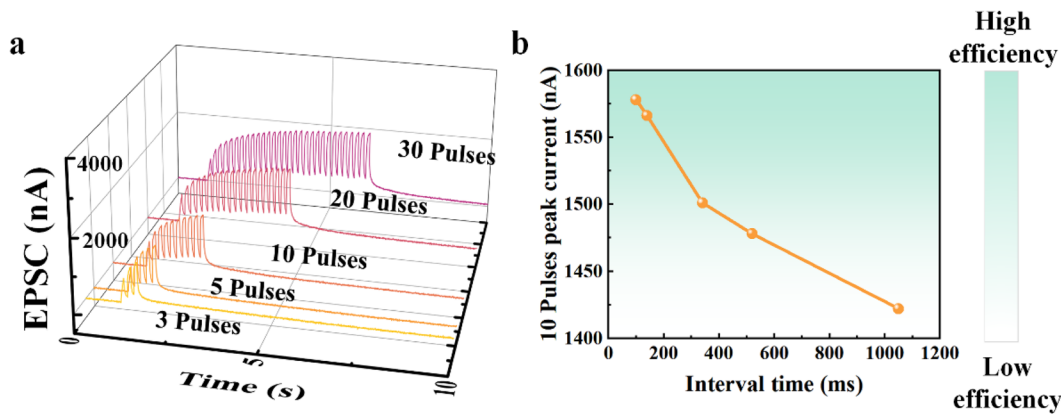


FIG. 5. (a) Short-term memory (STM) and long-term memory (LTM) of the device with multiple optical spikes. (b) The peak current response as a function of interval time with fixed ten pulses.

from traps and recombining over time. The process mimics the phenomenon that is observed in the biological nervous system, where residual Ca^{2+} from the previous stimulus promotes the transmission of transmitters, leading to pulse facilitation. In addition, temperature would also influence the decay time of the synaptic device, as shown in Fig. S4 (see in the supplementary material), which is mainly due to the accelerated thermal excitation of the carriers from the traps.⁴¹

In Fig. 4(a), the EPSC response was determined on synaptic plasticity with varying V_{GS} from -7 to -10 V by a step of 0.5 V ($V_{DS} = 0.5$ V, interval time of 100 ms). The EPSC response at -10 V is slightly higher than its corresponding value at -7 V. Figure 4(b) shows the relationship between the EPSC and gate voltage. With more negative gate voltage, the amplitude of the EPSC is larger, suggesting that the EPSC can be effectively modulated by gate bias. At an interval time of 100 ms, the EPSC peak current value increases from 618 nA at -7 V to 768 nA at -10 V. In Fig. 4(c), the EPSC values are shown to be elevated with increasing duration for each gate voltages. At a fixed V_{GS} of -9 V, the EPSC amplitude with duration time of 1000 s was measured to be 1704 nA, larger than the corresponding value of 693 nA with duration time of 100 s, due to the strengthening of optical excitation.

In Fig. 4(d), the drain tunability of synaptic plasticity was shown by varying the drain bias from 0.5 to 3.5 V. As the V_{DS} pulse amplitude rises, the EPSC amplitude exhibits a pronounced increase. This phenomenon means the recombination of photogenerated carriers and the carriers trapping process can be influenced by the drain voltage bias. As the V_{DS} increases from 0.5 to 3.5 V, as shown in Fig. 4(e), the EPSC enhances from 673 to 1459 nA, representing a notable improvement of over 117% . EPSC as a function of drain voltage is more evident than the case of varying gate voltages, indicating that V_{DS} plays a dominant role in determining the EPSC response compared to V_{GS} . As the duration of the drain bias increases, the EPSC amplitude gradually increases and then reaches the saturation value shown in Fig. 4(f), indicating that the amount of optically stimulated carrier is also approaching saturation. Therefore, the gate/drain bias can be used to modulate the EPSC response, which

adds a new dimension to fine-tune the response of optoelectronic synaptic AlGaIn/GaN MOS-HEMT.

In Fig. 5(a), the potentiation characteristics were monitored by varying the number of optical pulses from 3 pulses to 30 pulses. When a series of three optical pulses were applied, the synaptic device shows short-term persistence with a relatively low EPSC value. As the number of optical pulses increases, the amplitude of the final EPSC increases, indicating that the connection of a synapse in a biological neural network has also been consolidated. The final EPSC amplitude is 1117.5 nA with three pulses, whereas the EPSC amplitude increases to 1887.4 nA with 30 pulses. The apparent current increase in the EPSC amplitude suggests that the STM has transferred to LTM and the stronger synaptic weight modulation, which emulates the synapse functions.^{5,36} Information that would be quickly forgotten in the STM can be memorized as a long-term feature stored in the synaptic device through repeated stimulation/learning, which could be regulated by the learning interval time. As shown in Fig. 5(b), the effect of interval time on synaptic plasticity can also be demonstrated after ten optical pulses. When the pulse interval time increases from 100 to 1050 ms, the final EPSC after ten optical pulses decreases from 1578 to 1422 nA. Thus, an increase in the optical pulse interval time leads to weakened LTM, indicating that transition efficiency from STM to LTM could be well modulated by the interval time. In addition, this mechanism is consistent with the human brain's behavior for memory: when the learning intervals increase, the efficiency of memory will significantly reduce.

During the AlGaIn/GaN synaptic device operation, the device is applied with a V_{GS} lower than V_{TH} to electrically turn off the device. When the device is triggered by a single optical pulse, the photogenerated carriers are generated, which leads to a transient increase in the drain current. In addition, the carriers will be trapped at a shallow trap in the 2DEG channel or GaN buffer layer, corresponding to the STM. When the duration or the number of optical pulse is increased, the 2DEG channel of the AlGaIn/GaN heterojunction accumulated a large amount of photogenerated electrons, leading to an increase in the EPSC amplitude. Then, the electrons could

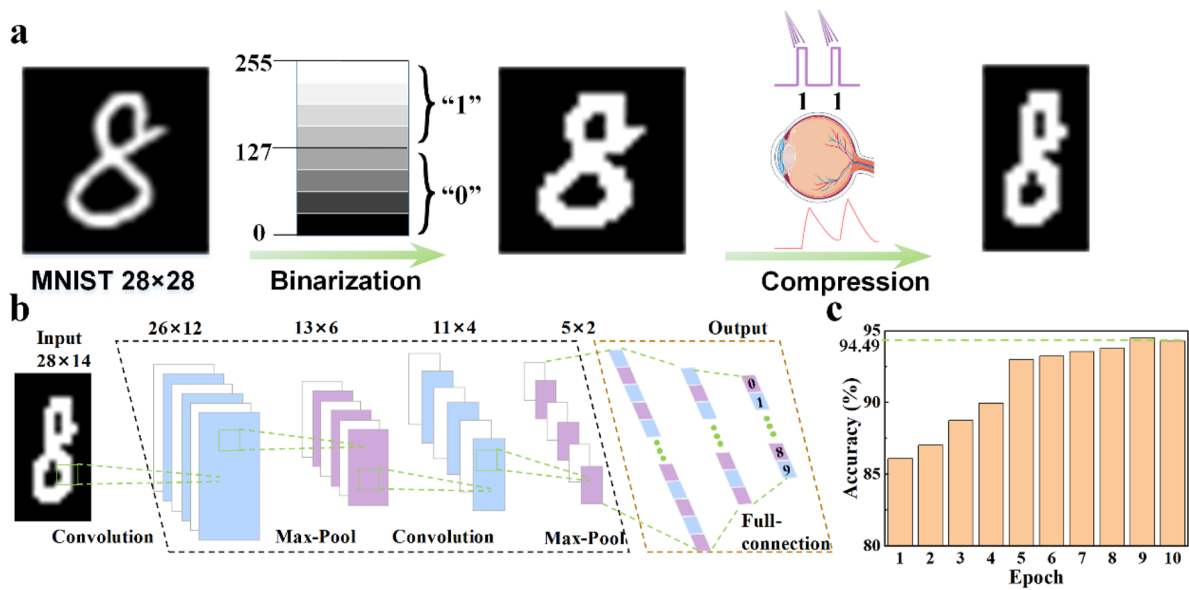


FIG. 6. (a) The 28×28 images in MNIST were compressed into 28×14 by optical pulses [00], [01], [10], and [11], where the pulse duration time is 300 ms and interval time is 250 ms. (b) The structure of the CNN model for verifying the preprocessing ability. (c) Recognition accuracy with training epochs.

TABLE I. Comparison of optoelectronic synaptic devices.

Device	Structure	Energy consumption	Application demonstration	References
AlGaIn/GaN MOS-HEMT	3-Terminal	34.2 pJ	Data preprocess and pattern recognition	This work
VO-FET	3-Terminal	4.8 nJ ^a	N/A	45
Silicon-nanocrystal transistors	2-Terminal	140 pJ	Pattern recognition	46
(Al, Ga)N NWs	2-Terminal	2.6 μ J	Pattern recognition	47
InAs NW	2-Terminal	35 nJ	N/A	48
ZTO/MgO memristor	2-Terminal	2.4 μ J ^a	Pattern recognition	49
Au/Cs ₂ AgBiBr ₆ /Au memristor	2-Terminal	0.4 nJ	Pattern recognition	50
2D Layered BiOI memristor	2-Terminal	220 nJ ^a	Pattern recognition	51

^aThe energy consumption is estimated using Eq. (1).

tunnel into Al₂O₃ dielectric and AlGaIn barrier layers and be trapped in deep-level traps.^{42,43} These trapped carriers take a longer time to release, corresponding to the LTM process of the device.

Processing the enormous amount of visual information received by the human eyes in real time represents an important daily routine task for our brains. Inspired by a recent study that human brain perceives the average of the preceding period at a specific moment,⁴⁴ AlGaIn/GaN synaptic devices were applied for preprocessing by optical pulse response. In this study, Modified National Institute of Standards and Technology (MNIST) validated the preprocessing ability of AlGaIn/GaN-based synapses. As shown in Fig. 6(a), the 28×28 images in the MNIST were binarized using a threshold of 127 gray-level, so the images consisted of “0” and “1,” as the signal “1” means a single light pulse and “0” means no light pulse. Each 2-bit code represents a specific current value, for example, [11] means two consecutive light pulses and [00] means no light pulse. Then, the binary images were compressed into 28×14 ,

where every two adjacent pixels in each row were encoded into one current value using the 2-bit signal of the AlGaIn/GaN synaptic device. To verify the image preprocessing ability, a convolution neural network (CNN) model was utilized, which consisted of two convolution layers, two Max-pool layers, and three full-connection layers, as shown in Fig. 6(b). The synapse devices act as a simulated 28×14 sensors array and then transmit the image information to the CNN as an input layer. Figure 6(c) shows the recognition accuracy of the testing dataset (10 000 testing images), which is about 94% after ten training epochs (60 000 training images), indicating that the data preprocessed by the AlGaIn/GaN synapse remains the main features. This approach simplifies the processing of visual input, allowing for more efficient cognitive functioning. In addition, halving the data volume results in accelerated processing and reduced energy consumption, demonstrating that the AlGaIn/GaN synapse device has huge potential for efficient information preprocessing.

Table I presents the comprehensive comparison with the optically stimulated synaptic transistors, nanowires, and memristors. The device in this study exhibits a much lower energy consumption, which is close to that of a biological synaptic event.⁵² Meanwhile, the synaptic device in this study shows great data preprocessing and pattern recognition ability. It is also worth noting that COMS compatibility of AlGaIn/GaN MOS-HEMT on the Si substrate in this study can be further fulfilled by shrinking the gate length⁵³ and employing an Au-free metal scheme⁵⁴ in the future investigation, which is beneficial for large-scale neuromorphic computing.

IV. CONCLUSION

In this work, an optoelectronic synaptic transistor based on the AlGaIn/GaN MOS-HEMT has been successfully demonstrated and investigated. Using 405 nm light pulse as stimulation, this optoelectronic synapse has successfully achieved EPSC, PPF, STM, and LTM. Within a single EPSC event, the energy consumption is only 34.2 pJ and the high SNR achieves 15.03 dB, which is beneficial for brain-inspired neuromorphic computing. Similar to the PPF effect of biological synapses, the PPF index of the AlGaIn/GaN synaptic device decreases with increasing interval time. For memory consolidation, the STM could be converted to LTM by increasing the number of optical spikes, showing a great potential for repetitive learning and memory. The gate/drain voltage enabled tunability of the EPSC has been well documented, adding a new dimension to fine-tune the synaptic weight. Moreover, a preprocessing system implemented by the synaptic device and enabled by the CNN algorithm was constructed for preprocessing input data, achieving a high recognition rate of over 94% after only ten epochs. In summary, this study demonstrates a low energy consumption AlGaIn/GaN MOS-HEMT synaptic device with highly adaptive tunability, which shows great potential for neuromorphic computing applications and massive data preprocessing applications.

SUPPLEMENTARY MATERIAL

See the supplementary material for more device properties, including writing-erasing characteristics, device-to-device/cycle-to-cycle uniformity, and decay time as a function of temperature.

ACKNOWLEDGMENTS

This work was supported by the ShanghaiTech University Startup Fund No. 2017F0203-000-14, the National Natural Science Foundation of China (Grant No. 52131303), the Natural Science Foundation of Shanghai (Grant No. 22ZR1442300), and, in part, by the CAS Strategic Science and Technology Program under Grant No. XDA18000000.

The authors would like to acknowledge technical support from ShanghaiTech Quantum Device Laboratory (SQDL).

AUTHOR DECLARATIONS

Conflict of Interest

The authors have no conflicts to disclose.

Author Contributions

Jiaxiang Chen and Haitao Du contributed equally to this work.

Jiaxiang Chen: Conceptualization (lead); Data curation (lead); Formal analysis (equal); Investigation (lead); Methodology (lead); Validation (lead); Writing – original draft (lead); Writing – review & editing (lead). **Haitao Du:** Conceptualization (lead); Data curation (lead); Formal analysis (equal); Investigation (lead); Methodology (lead); Software (lead); Validation (lead); Writing – original draft (lead); Writing – review & editing (lead). **Haolan Qu:** Conceptualization (equal); Data curation (equal); Validation (equal); Writing – review & editing (equal). **Han Gao:** Resources (equal); Writing – review & editing (equal). **Yitian Gu:** Resources (equal); Writing – review & editing (equal). **Yitai Zhu:** Methodology (equal); Writing – review & editing (equal). **Wenbo Ye:** Software (equal). **Jun Zou:** Supervision (supporting). **Hongzhi Wang:** Supervision (supporting). **Xinbo Zou:** Funding acquisition (lead); Investigation (lead); Methodology (lead); Resource (lead); Supervision (lead); Writing – review & editing (lead).

DATA AVAILABILITY

The data that support the findings of this study are available in GitHub, at <https://github.com/cjx24h/AlGaInGaIn-Synaptic-Devices>. The AlGaIn/GaN MOSHEMTs used in this study were designed, fabricated, and measured in ShanghaiTech University.

REFERENCES

- L. El Srouji, A. Krishnan, R. Ravichandran, Y. Lee, M. On, X. Xiao, and S. J. Ben Yoo, "Photonic and optoelectronic neuromorphic computing," *APL Photonics* 7(5), 051101 (2022).
- A. Mehonic and J. Eshraghian, "Brains and bytes: Trends in neuromorphic technology," *APL Mach. Learn.* 1, 020401 (2023).
- K. He, C. Wang, Y. He, J. Su, and X. Chen, "Artificial neuron devices," *Chem. Rev.* 123, 13796–13865 (2023).
- T. Leonard, S. Liu, H. Jin, and J. A. C. Incorvia, "Stochastic domain wall-magnetic tunnel junction artificial neurons for noise-resilient spiking neural networks," *Appl. Phys. Lett.* 122, 262406 (2023).
- M. Lee, S. Nam, B. Cho, O. Kwon, H. U. Lee, M. G. Hahm, U. J. Kim, and H. Son, "Accelerated learning in wide-band-gap AlN artificial photonic synaptic devices: Impact on suppressed shallow trap level," *Nano Lett.* 21, 7879–7886 (2021).
- N. Leroux, D. Marković, D. Sanz-Hernández, J. Trastoy, P. Bortolotti, A. Schulman, L. Benetti, A. Jenkins, R. Ferreira, J. Grollier, and F. A. Mizrahi, "Classification of multi-frequency RF signals by extreme learning, using magnetic tunnel junctions as neurons and synapses," *APL Mach. Learn.* 1, 036109 (2023).
- F. Zhou, Z. Zhou, J. Chen, T. H. Choy, J. Wang, N. Zhang, Z. Lin, S. Yu, J. Kang, H.-S. P. Wong, and Y. Chai, "Optoelectronic resistive random access memory for neuromorphic vision sensors," *Nat. Nanotechnol.* 14, 776–782 (2019).
- F. Zhou and Y. Chai, "Near-sensor and in-sensor computing," *Nat. Electron.* 3, 664–671 (2020).
- F. Liao, Z. Zhou, B. J. Kim, J. Chen, J. Wang, T. Wan, Y. Zhou, A. T. Hoang, C. Wang, J. Kang *et al.*, "Bioinspired in-sensor visual adaptation for accurate perception," *Nat. Electron.* 5, 84–91 (2022).
- D. Misra, "Special issue of interface on neuromorphic computing: An introduction and state of the field," *Electrochem. Soc. Interface* 32, 45 (2023).
- L. Q. Guo, H. Han, L. Q. Zhu, Y. B. Guo, F. Yu, Z. Y. Ren, H. Xiao, Z. Y. Ge, and J. N. Ding, "Oxide neuromorphic transistors gated by polyvinyl alcohol solid electrolytes with ultralow power consumption," *ACS Appl. Mater. Interfaces* 11, 28352–28358 (2019).

- ¹²N. Sghaier, N. Yacoubi, J. M. Bluet, A. Souifi, G. Guillot, C. Gaquiere, and J. C. De Jaeger, "Current instabilities and deep level investigation on AlGaIn/GaN HEMT's on silicon and sapphire substrates," in *Proceedings of the 16th International Conference on Microelectronics, Tunis, Tunisia, 6-8 December 2004* (IEEE, 2004).
- ¹³Y. Wang, L. Yin, W. Huang, Y. Li, S. Huang, Y. Zhu, D. Yang, and X. Pi, "Optoelectronic synaptic devices for neuromorphic computing," *Adv. Intell. Syst.* **3**, 2000099 (2020).
- ¹⁴X. Liu, D. Li, Y. Wang, D. Yang, and X. Pi, "Flexible optoelectronic synaptic transistors for neuromorphic visual systems," *APL Mach. Learn.* **1**, 031501 (2023).
- ¹⁵H. Liu, Y. Qin, H. Y. Chen, J. Wu, J. Ma, Z. Du, N. Wang, J. Zou, S. Lin, X. Zhang, Y. Zhang, and H. Wang, "Artificial neuronal devices based on emerging materials: Neuronal dynamics and applications," *Adv. Mater.* **35**, e2205047 (2023).
- ¹⁶M. Xu, X. Chen, Y. Guo, Y. Wang, D. Qiu, X. Du, Y. Cui, X. Wang, and J. Xiong, "Reconfigurable neuromorphic computing: Materials, devices, and integration," *Adv. Mater.* **35**, e2301063 (2023).
- ¹⁷P. A. Merolla, J. V. Arthur, R. Alvarez-Icaza, A. S. Cassidy, J. Sawada, F. Akopyan, B. L. Jackson, N. Imam, C. Guo, Y. Nakamura, B. Brezzo, I. Vo, S. K. Esser, R. Appuswamy, B. Taba, A. Amir, M. D. Flickner, W. P. Risk, R. Manohar, and D. S. Modha, "A million spiking-neuron integrated circuit with a scalable communication network and interface," *Science* **345**, 668–673 (2014).
- ¹⁸Y. B. Guo, L. Q. Zhu, W. T. Gao, Z. Y. Ren, H. Xiao, and Z. Y. Ge, "Low-voltage protonic/photonic synergic coupled oxide phototransistor," *Org. Electron.* **71**, 31–35 (2019).
- ¹⁹L. Yin, W. Huang, R. Xiao, W. Peng, Y. Zhu, Y. Zhang, X. Pi, and D. Yang, "Optically stimulated synaptic devices based on the hybrid structure of silicon nanomembrane and perovskite," *Nano Lett.* **20**, 3378–3387 (2020).
- ²⁰Y. T. Li, J. Z. Li, L. Ren, K. Xu, S. Chen, L. Han, H. Liu, X. L. Guo, D. L. Yu, D. H. Li, L. Ding, L. M. Peng, and T. L. Ren, "Light-controlled reconfigurable optical synapse based on carbon nanotubes/2D perovskite heterostructure for image recognition," *ACS Appl. Mater. Interfaces* **14**, 28221–28229 (2022).
- ²¹J. Bisquert, A. Bou, A. Guerrero, and E. Hernández-Balaguera, "Resistance transient dynamics in switchable perovskite memristors," *APL Mach. Learn.* **1**, 036101 (2023).
- ²²Y. Shi, X. Liang, B. Yuan, V. Chen, H. Li, F. Hui, Z. Yu, F. Yuan, E. Pop, H. S. P. Wong, and M. Lanza, "Electronic synapses made of layered two-dimensional materials," *Nat. Electron.* **1**, 458–465 (2018).
- ²³X. Hua, J. Zheng, X. Han, Z. Hao, Y. Luo, C. Sun, Y. Han, B. Xiong, J. Wang, H. Li, L. Gan, M. Al Khalifioui, J. Brault, and L. Wang, "Artificial optoelectronic synapse with nanolayered GaN/AlN periodic structure for neuromorphic computing," *ACS Appl. Nano Mater.* **6**, 8461–8467 (2023).
- ²⁴C. Kai, Y. Wang, X. Liu, X. Liu, X. Zhang, X. Pi, and D. Yang, "AlGaIn/GaN-based optoelectronic synaptic devices for neuromorphic computing," *Adv. Opt. Mater.* **11**, 2202105 (2023).
- ²⁵J. Chen, M. Zhu, X. Lu, and X. Zou, "Electrical characterization of GaN Schottky barrier diode at cryogenic temperatures," *Appl. Phys. Lett.* **116**, 062102 (2020).
- ²⁶Y. Zhang, Y. Gu, J. Chen, Y. Zhu, B. Chen, H. Jiang, K. M. Lau, and X. Zou, "Small V_{th} shift and low dynamic R_{on} in GaN MOSHEMT with ZrO_2 gate dielectric," *IEEE Trans. Electron Devices* **70**, 5590–5595 (2023).
- ²⁷Y. Zhang, L. Xu, Y. Gu, H. Guo, H. Jiang, K. M. Lau, and X. Zou, "Dynamic characteristics of GaN MISHEMT with 5-nm *in-situ* SiN_x dielectric layer," *IEEE J. Electron Devices Soc.* **10**, 540–546 (2022).
- ²⁸J. Chen, W. Huang, H. Qu, Y. Zhang, J. Zhou, B. Chen, and X. Zou, "Study of minority carrier traps in p-GaN gate HEMT by optical deep level transient spectroscopy," *Appl. Phys. Lett.* **120**, 212105 (2022).
- ²⁹A. A. Istratov and O. F. Vyvenko, "Exponential analysis in physical phenomena," *Rev. Sci. Instrum.* **70**, 1233–1257 (1999).
- ³⁰Y. Mo, B. Luo, H. Dong, and B. Hou, "Light-stimulated artificial synapses based on Si-doped GaN thin films," *J. Mater. Chem. C* **10**, 13099–13106 (2022).
- ³¹C. Li, X. Zhang, P. Chen, K. Zhou, J. Yu, G. Wu, D. Xiang, H. Jiang, M. Wang, and Q. Liu, "Short-term synaptic plasticity in emerging devices for neuromorphic computing," *iScience* **26**, 106315 (2023).
- ³²W. Shi, S. Huang, X. Wang, Q. Jiang, Y. Yao, L. Bi, Y. Li, K. Deng, J. Fan, H. Yin *et al.*, "Low-thermal-budget Au-free ohmic contact to an ultrathin barrier AlGaIn/GaN heterostructure utilizing a micro-patterned ohmic recess," *J. Semicond.* **42**, 092801 (2021).
- ³³D. Hao, D. Liu, J. Zhang, Y. Wang, and J. Huang, "Lead-free perovskites-based photonic synaptic devices with logic functions," *Adv. Mater. Technol.* **6**, 2100678 (2021).
- ³⁴S. Gao, G. Liu, H. Yang, C. Hu, Q. Chen, G. Gong, W. Xue, X. Yi, J. Shang, and R. W. Li, "An oxide Schottky junction artificial optoelectronic synapse," *ACS Nano* **13**, 2634–2642 (2019).
- ³⁵Y. Gu, Y. Wang, J. Chen, B. Chen, M. Wang, and X. Zou, "Temperature-dependent dynamic degradation of carbon-doped GaN HEMTs," *IEEE Trans. Electron Devices* **68**, 3290–3295 (2021).
- ³⁶S. Wen, J. Li, Z. Wang, Z. Zhang, and J. Zhang, "Low-power and high PPF feature synaptic transistors with 3D interface based on SnO_2 nanofibers for neuromorphic application," *Appl. Phys. Lett.* **123**, 043503 (2023).
- ³⁷C. K. Shen, R. Chaurasiya, K. T. Chen, and J. S. Chen, "Synaptic emulation via ferroelectric P(VDF-TrFE) reinforced charge trapping/detrapping in zinc-tin oxide transistor," *ACS Appl. Mater. Interfaces* **14**, 16939–16948 (2022).
- ³⁸J. Wen, L. Q. Zhu, Y. M. Fu, H. Xiao, L. Q. Guo, and Q. Wan, "Activity dependent synaptic plasticity mimicked on indium-tin-oxide electric-double-layer transistor," *ACS Appl. Mater. Interfaces* **9**, 37064–37069 (2017).
- ³⁹R. D. Burgoyne, "Neuronal calcium sensor proteins: Generating diversity in neuronal Ca^{2+} signalling," *Nat. Rev. Neurosci.* **8**, 182–193 (2007).
- ⁴⁰Y. Zhu, G. Liu, Z. Xin, C. Fu, Q. Wan, and F. Shan, "Solution-processed, electrolyte-gated In_2O_3 flexible synaptic transistors for brain-inspired neuromorphic applications," *ACS Appl. Mater. Interfaces* **12**, 1061–1068 (2020).
- ⁴¹M. Reshchikov and H. Morkoç, "Luminescence from defects in GaN," *Physica B* **376–377**, 428–431 (2006).
- ⁴²B. Sarkar, N. Ramanan, S. Jayanti, N. D. Spigna, B. Lee, P. Franzon, and V. Misra, "Dual floating gate unified memory MOSFET with simultaneous dynamic and non-volatile operation," *IEEE Electron Device Lett.* **35**, 48–50 (2014).
- ⁴³J. Chen, H. Qu, J. Sui, X. Lu, and X. Zou, "Relaxation kinetics of interface states and bulk traps in atomic layer deposited $ZrO_2/\beta\text{-Ga}_2O_3$ metal-oxide-semiconductor capacitors," *J. Appl. Phys.* **135**, 085702 (2024).
- ⁴⁴M. Manassi, A. Liberman, W. Chaney, and D. Whitney, "The perceived stability of scenes: Serial dependence in ensemble representations," *Sci. Rep.* **7**, 1971 (2017).
- ⁴⁵C. Gao, H. Yang, E. Li, Y. Yan, L. He, H. Chen, Z. Lin, and T. Guo, "Heterostructured vertical organic transistor for high-performance optoelectronic memory and artificial synapse," *ACS Photonics* **8**, 3094–3103 (2021).
- ⁴⁶L. Yin, C. Han, Q. Zhang, Z. Ni, S. Zhao, K. Wang, D. Li, M. Xu, H. Wu, X. Pi, and D. Yang, "Synaptic silicon-nanocrystal phototransistors for neuromorphic computing," *Nano Energy* **63**, 103859, (2019).
- ⁴⁷M. Zhou, Y. Zhao, X. Gu, Q. Zhang, J. Zhang, M. Jiang, and S. Lu, "Realize low-power artificial photonic synapse based on (Al,Ga)N nanowire/graphene heterojunction for neuromorphic computing," *APL Photonics* **8**, 076107 (2023).
- ⁴⁸B. Li, W. Wei, X. Yan, X. Zhang, P. Liu, Y. Luo, J. Zheng, Q. Lu, Q. Lin, and X. Ren, "Mimicking synaptic functionality with an InAs nanowire phototransistor," *Nanotechnology* **29**, 464004 (2018).
- ⁴⁹C.-C. Hsu, S. Shrivastava, S. Pratik, S. Chandrasekaran, and T.-Y. Tseng, "ZTO/MgO-based optoelectronic synaptic memristor for neuromorphic computing," *IEEE Trans. Electron Devices* **70**, 1048–1054 (2023).
- ⁵⁰Q. Sun, Z. Guo, X. Zhu, Q. Jiang, H. Liu, X. Liu, C. Sun, Y. Zhang, L. Wu, and R.-W. Li, "Optogenetics-inspired manipulation of synaptic memory using all-optically controlled memristors," *Nanoscale* **15**, 10050–10056 (2023).
- ⁵¹P. Lei, H. Duan, L. Qin, X. Wei, R. Tao, Z. Wang, F. Guo, M. Song, W. Jie, and J. Hao, "High-performance memristor based on 2d layered BiOI nanosheet for low-power artificial optoelectronic synapses," *Adv. Funct. Mater.* **32**, 2201276 (2022).
- ⁵²Y. Van De Burgt, E. Lubberman, E. J. Fuller, S. T. Keene, G. C. Faria, S. Agarwal, M. J. Marinella, A. Alec Talin, and A. Salleo, "A non-volatile organic electrochemical device as a low-voltage artificial synapse for neuromorphic computing," *Nat. Mater.* **16**, 414–418 (2017).
- ⁵³S. Lei, W.-C. Cheng, J. Wu, L. Wang, Q. Wang, G. Xia, F. Zhao, and H. Yu, "Low leakage GaN HEMTs with sub-100 nm T-shape gates fabricated by a low-damage etching process," *J. Mater. Sci.: Mater. Electron.* **31**, 5886–5891 (2020).
- ⁵⁴V. Garbe, S. Seidel, A. Schmid, U. Bläß, E. Meissner, and J. Heitmann, "Ultra-low resistance Au-free V/Al/Ti/TiN ohmic contacts for AlGaIn/GaN HEMTs," *Appl. Phys. Lett.* **123**, 203506 (2023).